Ultra-broad and sharp-transition bandpass terahertz filters by hybridizing multiple resonances mode in monolithic metamaterials

Ting-Tso Yeh,[1,4] Simone Genovesi,[2,3,4] Agostino Monorchio,[2] Enrico Prati,[3] Filippo Costa,[2] Tsung-Yu Huang,[1] and Ta-Jen Yen[1,*]

[1]*Department of Materials Science and Engineering, National Tsing Hua University, Hsinchu, Taiwan*
[2]*Dipartimento Ingegneria dell'Informazione, Università di Pisa, Via G. Caruso 16, Pisa, 56122, Italy*
[3]*Laboratorio MDM, Istituto per la Microelettronica e i Microsistemi, Consiglio Nazionale delle Ricerche (CNR), Via Olivetti 2, 20041, Agrate Brianza (MI), Italy*
[4]*These authors contributed equally to this work.*
**tjyen@mx.nthu.edu.tw*

Abstract: We present three monolithic metamaterial-based THz bandpass filters, the skewed circular slot rings, meandered slots and Jerusalem cross slots, to fit in the THz gap. These THz bandpass filters are comprised of a metal-dielectric-metal (MDM) structure that supports multiple resonances of electric dipole, magnetic dipole, and standing-wave-like modes. By exciting and further hybridizing these individual resonance modes, we demonstrate excellent performance of broad bandwidth and sharp band-edge transition beyond conventional bandpass filters. By further employing our ad hoc Genetic Algorithm (GA) and Periodic Method of Moments (PMM) to optimize our designs, we achieve an ultra-broad 3dB fractional bandwidth and sharp band-edge transition up to 82.2% and 58.3 dB/octave, respectively, benefiting the practical applications such as material recognition in security systems, imaging, and absorbers.

OCIS codes: (160.3918) Metamaterials; (230.7408) Wavelength filtering devices; (230.4000) Microstructure fabrication.

References and links

1. N. Seddon and T. Bearpark, "Observation of the inverse Doppler effect," Science **302**(5650), 1537–1540 (2003).
2. J. Lu, T. M. Grzegorczyk, Y. Zhang, J. Pacheco, Jr., B. I. Wu, J. A. Kong, and M. Chen, "Cerenkov radiation in materials with negative permittivity and permeability," Opt. Express **11**(7), 723–734 (2003).
3. R. A. Shelby, D. R. Smith, and S. Schultz, "Experimental verification of a negative index of refraction," Science **292**(5514), 77–79 (2001).
4. W. S. Cai, U. K. Chettiar, A. V. Kildishev, and V. M. Shalaev, "Optical cloaking with metamaterials," Nat. Photonics **1**(4), 224–227 (2007).
5. X. Zhang and Z. W. Liu, "Superlenses to overcome the diffraction limit," Nat. Mater. **7**(6), 435–441 (2008).
6. H. Wakatsuchi, S. Greedy, C. Christopoulos, and J. Paul, "Customised broadband metamaterial absorbers for arbitrary polarisation," Opt. Express **18**(21), 22187–22198 (2010).
7. K. L. Tsakmakidis, A. D. Boardman, and O. Hess, "'Trapped rainbow' storage of light in metamaterials," Nature **450**(7168), 397–401 (2007).
8. H. T. Chen, W. J. Padilla, J. M. O. Zide, A. C. Gossard, A. J. Taylor, and R. D. Averitt, "Active terahertz metamaterial devices," Nature **444**(7119), 597–600 (2006).
9. B. Ferguson and X. C. Zhang, "Materials for terahertz science and technology," Nat. Mater. **1**(1), 26–33 (2002).
10. M. R. Leahy-Hoppa, M. J. Fitch, X. Zheng, L. M. Hayden, and R. Osiander, "Wideband terahertz spectroscopy of explosives," Chem. Phys. Lett. **434**(4-6), 227–230 (2007).
11. J. F. Federici, B. Schulkin, F. Huang, D. Gary, R. Barat, F. Oliveira, and D. Zimdars, "THz imaging and sensing for security applications—explosives, weapons and drugs," Semicond. Sci. Technol. **20**(7), S266–S280 (2005).
12. D. M. Mittleman, M. Gupta, R. Neelamani, R. G. Baraniuk, J. V. Rudd, and M. Koch, ""Recent advances in terahertz imaging," Appl. Phys. B-Lasers Opt. **68**(6), 1085–1094 (1999).
13. B. B. Hu and M. C. Nuss, "Imaging with terahertz waves," Opt. Lett. **20**(16), 1716–1718 (1995).
14. F. Miyamaru, Y. Saito, M. Takeda, B. Hou, L. Liu, W. Wen, and P. Sheng, "Terahertz electric response of fractal metamaterial structures," Phys. Rev. B **77**(4), 045124 (2008).

#162148 - $15.00 USD Received 27 Jan 2012; revised 1 Mar 2012; accepted 13 Mar 2012; published 19 Mar 2012

15. D. R. Chowdhury, R. Singh, M. Reiten, H. T. Chen, A. J. Taylor, J. F. O'Hara, and A. K. Azad, "A broadband planar terahertz metamaterial with nested structure," Opt. Express **19**(17), 15817–15823 (2011).
16. N. R. Han, Z. C. Chen, C. S. Lim, B. Ng, and M. H. Hong, "Broadband multi-layer terahertz metamaterials fabrication and characterization on flexible substrates," Opt. Express **19**(8), 6990–6998 (2011).
17. M. Z. Lu, W. Z. Li, and E. R. Brown, "Second-order bandpass terahertz filter achieved by multilayer complementary metamaterial structures," Opt. Lett. **36**(7), 1071–1073 (2011).
18. M. Al-Joumayly and N. Behdad, "A New Technique for Design of Low-Profile, Second-Order, Bandpass Frequency Selective Surfaces," IEEE Trans. Antenn. Propag. **57**(2), 452–459 (2009).
19. S. Genovesi, T. Yen, A. Monorchio, E. Prati, Y. Chiang, and F. Costa, "Optimization of wide-bandpass filter within the Terahertz frequency regime," in Proceedings of XXXth URSI General Assembly and Scientific Symposium, (2011), pp. 1–4.
20. D. S. Weile and E. Michielssen, "Genetic algorithm optimization applied to electromagnetics: A review," IEEE Trans. Antenn. Propag. **45**(3), 343–353 (1997).
21. T. K. Wu, *Frequency selective surface and grid array*, (John Wiley & Sons, 1995).
22. G. Dolling, C. Enkrich, M. Wegener, J. F. Zhou, C. M. Soukoulis, and S. Linden, "Cut-wire pairs and plate pairs as magnetic atoms for optical metamaterials," Opt. Lett. **30**(23), 3198–3200 (2005).
23. J. F. Zhou, E. N. Economon, T. Koschny, and C. M. Soukoulis, "Unifying approach to left-handed material design," Opt. Lett. **31**(24), 3620–3622 (2006).
24. S. T. Chase and R. D. Joseph, "Resonant array bandpass filters for the far infrared," Appl. Opt. **22**(11), 1775–1779 (1983).
25. S. Zhang, W. J. Fan, K. J. Malloy, S. R. J. Brueck, N. C. Panoiu, and R. M. Osgood, "Near-infrared double negative metamaterials," Opt. Express **13**(13), 4922–4930 (2005).
26. V. A. Fedotov, M. Rose, S. L. Prosvirnin, N. Papasimakis, and N. I. Zheludev, "Sharp trapped-mode resonances in planar metamaterials with a broken structural symmetry," Phys. Rev. Lett. **99**(14), 147401 (2007).
27. N. Papasimakis, V. A. Fedotov, N. I. Zheludev, and S. L. Prosvirnin, "Metamaterial analog of electromagnetically induced transparency," Phys. Rev. Lett. **101**(25), 253903 (2008).

1. Introduction

Metamaterials are artificially constructed sub-wavelength structures, which have increasingly attracted immense attention caused by their unprecedented electromagnetic properties such as negative permittivity, negative permeability and negative refractive index media [1–3] to control light propagation for various purposes, such as invisible cloaking [4], superlensing [5], perfect absorbers [6] and light trapping [7]. In fact, metamaterials exhibit scalable properties beyond naturally existing materials to offer the aforementioned properties within a wide range of frequencies from microwaves towards visible regions, especially within the so-called terahertz gap (THz gap) [8]. By means of metamaterials, so far researchers have demonstrated several THz devices for various applications, including security systems [9–11], imaging [12, 13] and perfect absorbers [6]. Although metamaterials enable new electromagnetic properties, their operating bandwidth is typically narrow due to their resonance nature, and such a narrow operation bandwidth considerably impedes the employment of metamaterials in many practical applications. To broaden the limited bandwidth of metamaterials, a promising solution is to hybridize multiple resonances in carefully designed metamaterials [14–19]. Within this framework, it is interesting to notice that a great attention has been devoted to the design of bandstop THz filters whereas less attention has been dedicated to THz bandpass dichroics [17, 18] that are required in a wide range of applications.

As a consequence, here we design three monolithic metamaterials comprised of metal-dielectric-metal (MDM) structures to demonstrate THz bandpass filters. The first demonstration is the skewed circular slot rings, which support multiple resonance modes including magnetic dipole resonance, electric dipole resonance and standing-wave-like resonance, respectively. By hybridizing multiple resonances in the designed skewed circular slot rings, we superimpose a couple of allowed bands together, realizing an unusual bandpass filter with a broad bandwidth of 51.7% and sharp band-edge transitions of 13.9 dB/octave for the lower band edge and 30.2 dB/octave for the higher band edge, but meanwhile with an excellent transmittance efficiency up to 80% in the THz region. In addition, to further engineer the desired performance, for example, broader bandwidth or sharper transition, we optimize the transmission profiles of these metamaterial-based filters by developing a stochastic procedure of the ad hoc genetic algorithm (GA) [20] in conjunction with a periodic

#162148 - $15.00 USD Received 27 Jan 2012; revised 1 Mar 2012; accepted 13 Mar 2012; published 19 Mar 2012

method of moments (PMM) [21]. Resting on our optimization process, we demonstrate two more compact THz bandpass filters, the meandered slots and the Jerusalem crosses. The former show an ultra-broad bandwidth up to 80%, and the latter display sharper band-edge transition up to 58.3 dB/octave, respectively. All three monolithic metamaterial-based THz bandpass filters significantly surpass other multi-layer or multi-element designs [14–16].

2. Sample fabrication and measurement

All three designed THz bandpass filters were fabricated by a standard UV photolithographic process with a double-side alignment step and by a lift-off process. To fabricate these three monolithic metamaterial-based THz bandpass filters, first we employed a vacuum tape to fix a Mylar film of 38 μm thick on a silicon wafer. Here, the flexible Mylar film is a transparent substrate within our interested THz region, and the rigid silicon wafer serves as a carrier through. Next, we spun a 1.4 μm-thick layer of photoresist (AZ5214) on the Mylar film, introduced the designed patterns by a UV photolithographic process, and deposited a 200-nm-thick cooper layer by an electron beam evaporator. After finishing these photolithography and deposition steps, we immersed the specimens in an acetone solution to lift off the excessive cooper layer by a step of ultrasonication bath, leaving the defined cooper pattern on one side of Mylar film. Besides, to fabricate the cooper pattern on the other side of Mylar film, we removed the Mylar film with the one-side cooper pattern from the silicon wafer, flipped the Mylar film and attached it on a silicon wafer again. Then, we conducted the second photolithographic process with an extra step of double-side alignment, to align the second pattern with the first one on both sides of the Mylar film. Finally, we repeated the deposition process and the lift-off process aforementioned to fabricate the second layer of the defined cooper pattern, completing the monolithic metamaterial-based THz bandpass filters of a sandwiched metal-dielectric-metal (MDM) structure. After successfully fabricating the MDM structures, we utilized a Fourier transform infrared spectrometer (Bruker Vertex 70V FTIR) to measure the relative transmittance of the metamaterial-based THz bandpass filters. These filters were illuminated by a mercury lamp through an aperture of 8 mm in diameter, and a Si THz detector was placed on the opposite side to collect the transmitted signals. All measurements were done in vacuum to reduce the noise from the ambient environment including the absorption by moisture and air.

3. Experiment results and discussions of the skewed circular slot ring

The unit cell of the skewed circular slot rings is presented in Fig. 1(a), and the translation vectors are $t_1 = 70\ \mu m\ \hat{a}$ and $t_2 = 70\ \mu m\ \hat{b}$ (the angle between the two axis, a and b, is 60°) to construct a 2-D lattice. Two cooper layers of the skewed circular slot rings sandwich a THz-transparent Mylar substrate, giving rise to a metal-dielectric-metal (MDM) structure. In fact, these skewed circular slot rings consist of two constituent components: the inner MDM (MDM-I) and the outer MDM (MDM-O), as shown in Fig. 1(b). To examine the electromagnetic properties of these two constituent component and their coupling effects, we simulated the MDM-I, the MDM-O, and the integrated MDM to investigate the respective resonance modes by employing three-dimensional full-wave simulation software *CST Microwave Studio*^{TM}. First, the transmission and reflection spectra attributed to the MDM-I are shown in Fig. 2(a), indicating an anti-symmetric resonance mode at $f_m = 1.19$ THz and a symmetric resonance mode at $f_e = 3.01$ THz [22, 23]. Next, the MDM-O exhibits two passbands at $f_{sw1} = 1.54$ THz and $f_{sw2} = 3.34$ THz, as shown in Fig. 2(b), which are due to standing-wave-like resonance and magnetic dipolar resonance, respectively [24, 25]. Finally, by integrating the MDM-I and the MDM-O together to create the composite MDM structure of the skewed circular slot rings, we observed that this composite MDM presents two responses at $f_{t1} = 1.04$ THz and $f_{t2} = 1.41$ THz as presented in Fig. 2(c), which stem from the mode coupling between the MDM-I and MDM-O components and present an unusual THz

#162148 - $15.00 USD Received 27 Jan 2012; revised 1 Mar 2012; accepted 13 Mar 2012; published 19 Mar 2012

bandpass filter with the excellent performance of great transmittance efficiency, broad bandwidth, and sharp band-edge transition.

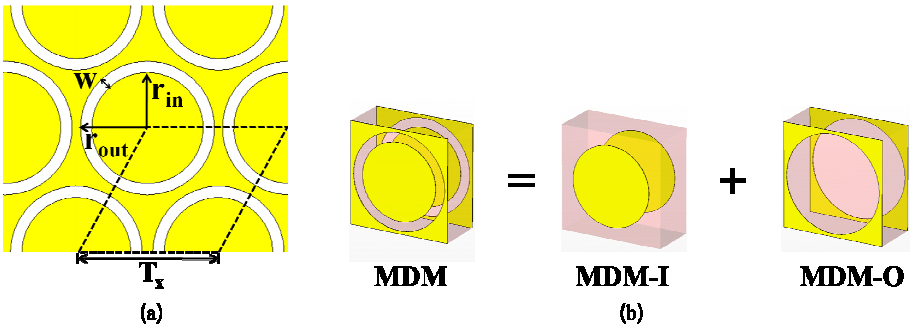

Fig. 1. (a) The shapes and dimensions of the skewed circular slot ring; T_x = 70 μm, W = 13 μm, r_{in} = 27 μm, and r_{out} = 32.5 μm when the dashed parallelogram indicates the unit cell of the skewed circular slot ring. (b) Unit cell of the proposed three MDM, which consists of two components: MDM-I and MDM-O.

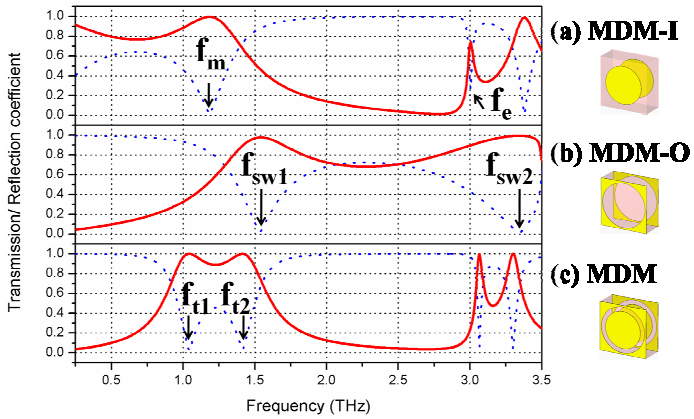

Fig. 2. Simulated transmission (red solid lines) and reflection (blue dotted lines) spectra of (a) MDM-I, (b) MDM-O, and (c) the MDM of the skewed circular slot ring sample. For all structures, the Mylar substrates are assumed lossless.

To further interpret those resonance modes shown in Fig. 2, we scrutinized the distribution of surface currents at the aforementioned resonance frequencies of interest. The surface currents on MDM-I of the circular slot ring sample are shown in Fig. 3(a). At f_m = 1.19 THz, an anti-symmetric mode exists between the top layer and the bottom layer, resulting in a magnetic dipolar resonance; at f_e = 3.01 THz, a symmetric mode appears between the top layer and the bottom layer, resulting in an electric resonance instead. Besides, for MDM-O component, at f_{sw1} = 1.54 THz and at f_{sw2} = 3.34 THz the surface currents oscillate in the form of standing waves along the perimeter of the circular slot, as shown in Fig. 3(b).

By hybridizing MDM-I and MDM-O together to assemble the skewed circular slot rings, we realize complex electromagnetic properties as seen previously in Fig. 2. Figure 3(c) reveals distinct surface-current distributions of the skewed circular slot rings at the two respective resonant frequencies. First, at the resonance f_{t1} = 1.04 THz of the composite MDM structure, the currents on these two constituent components oscillate in counter direction to each other with almost the same magnitude. Therefore, these induced surface currents interfere destructively corresponding to a so-called "trapped-mode resonance" that stems from mode coupling between the symmetry mode f_e from MDM-I and the standing-wave-like mode f_{sw1} from MDM-O, leading to an allowed band [26, 27]. Second, at another resonance f_{t2} =

#162148 - $15.00 USD Received 27 Jan 2012; revised 1 Mar 2012; accepted 13 Mar 2012; published 19 Mar 2012

1.41 THz of the MDM, the induced currents oscillate in opposite directions in both layers, resulting in another trapped-mode resonance due to the mode coupling between the asymmetry mode f_m from MDM-I and the standing-wave-like mode f_{sw2} from MDM-O, leading to the second allowed band. Eventually, these two allowed bands merge together, giving rise to a broad bandpass filter in THz region.

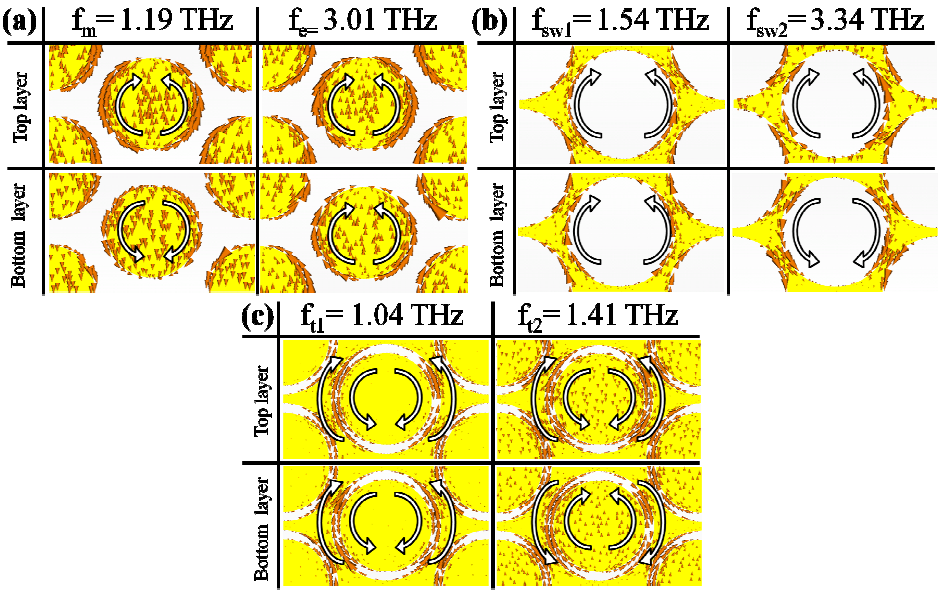

Fig. 3. Simulated induced-surface-current distributions of (a) MDM-I at 1.19 THz and 3.01 THz, (b) MDM-O at 1.54 THz and 3.34 THz, and (c) the MDM at 1.04 THz and 1.41 THz. The yellow parts indicate the metallic layer, copper, and the orange cones display the directions of the induced surface-currents.

Finally, the fabricated skewed circular slot rings and their corresponding measured responses were shown in Fig. 4. As expected, our designed monolithic metamaterial-based filter structure exhibits a broad fractional bandwidth of 51.7%, and the band-edge transitions have been evaluated as well in which the lower and upper skirts of the transmission profile are 13.3 dB/oct and 30.2 dB/oct, respectively. Both the measurement and simulation results are in excellent agreement, demonstrated beyond conventional THz bandpass filters. To summarize, by hybridizing the resonances in different components and coupling them together, which is sensitive to the geometric parameters of the designed structure, we can obtain a broadband and compact filter. To further engineer the desired performance, for example, broader bandwidth or sharper transition, we need to change the geometry of the structure, which is a challenging task. As a result, to achieve the desired broader fractional bandwidth and sharper transition, we developed a stochastic procedure of the ad hoc genetic algorithm (GA) in conjunction with a periodic method of moments (PMM) rather than a trial-and-error process, whose detail will be described in section 4.1. By means of our GA code, we obtained two more designed structures to effectively satisfy the broader fractional bandwidth by the meandered slots, and the sharper transition by the Jerusalem crosses, respectively. The corresponding results will be presented in section 4.2.

#162148 - $15.00 USD Received 27 Jan 2012; revised 1 Mar 2012; accepted 13 Mar 2012; published 19 Mar 2012

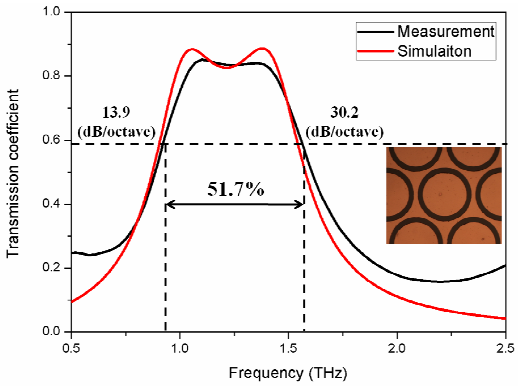

Fig. 4. The transmittance spectra of the skewed circular slot ring. The inset shows the optical microscopic (OM) image of the fabricated sample.

4. Optimized performance by ad hoc genetic algorithm

4.1 GA-based optimization process

The genetic algorithm is one of the most widespread evolutionary algorithms that basically mimics the Darwinian notion of the survival of the fittest guaranteed by natural selection and evolution. In our GA implementation all the parameters which require optimization are encoded into a binary-encoded chromosome $\underline{x}$. The chromosome comprises all the necessary information for describing a candidate solution of the investigated problem. A set of chromosomes forms a population and the aim of the algorithm is to improve this population at each iteration, in order to satisfy a criterion imposed by the designer. This task can be formulated by considering a function $F(\underline{x})$ (commonly referred as the *fitness function*), which describes the performance of chromosome $\underline{x}$. Depending on the problem, the objective is to find the $\underline{x}$ which minimizes or maximizes $F(\underline{x})$. Each chromosome is tested by the fitness function three operators (selection, crossover and mutation) are responsible for driving the evolution achieve the imposed goal [19].We have set the dimension of the population to 32 chromosomes and we have imposed 1000 generations as a criterion for stopping the evolution. This means we have 32000 calls to the PMM electromagnetic solver for the overall evolution. The complete flow-chart is illustrated in 5(a).

In this work, we developed an ad hoc GA code to optimize the desired performance including ultra broad width and sharp edge transition. More in detail, in our optimization procedure, the design variables encoded in the chromosome are the thickness d of the Mylar substrate, the periodicity T_x of the square lattice and the shape printed on the unit cell. Moreover, we impose constraints on the dielectric thickness d, which is assumed from 10 μm to 38 μm with 2 μm step, 14 different variables, and also on the resolution of the unit cell shape for the practical fabrication process we can achieve. The shape of the unit cell of the periodic surface is encoded by using a 16 x 16 binary mask where '1' means presence of metal and '0' is associated to only the dielectric, as shown in Fig. 5(b). We imposed a four-fold symmetry to the periodic element to obtain polarization-independent frequency responses. The employed fitness function that has to be minimized for the ultra-broad fractional bandwidth is reported in Eq. (1) whereas the criterion for the sharp band-edge transition is expressed by Eq. (2):

$$F_1 = avg\left[A - T(f)\big|_{f\in Br}\right] - \left(B - \max\left(T(f)\big|_{f\in Rr}\right)\right), \qquad (1)$$

#162148 - $15.00 USD Received 27 Jan 2012; revised 1 Mar 2012; accepted 13 Mar 2012; published 19 Mar 2012

$$F_2 = c_1 \left\{ avg\left[A - T(f)\big|_{f \in Br} \right] \right\} + c_2 \left\{ -\alpha + \beta - \left(B - \max\left(T(f)\big|_{\substack{f<F_3 \\ f>F_4}} \right) \right) \right\}. \qquad (2)$$

In Eq. (1) the transmission coefficient $T(f)$ has to be as close as possible in average (avg) to the desired level A (A = 1 in our case) within the bandapss region (Br) and it has to stay below level B (B = 0.2 in our case) in the rejection region (Rr). In Eq. (2) we are more concerned about the steepness of the band-edge transitions (α, β) therefore we relax the requirement of a large bandpass in favor of a faster decay of $T(f)$ by imposing $c_1 < c_2$ (c_1 = 0.3, c_2 = 0.7 in our case).

It is worth mentioning that the frequency response of the unit cell has been evaluated by the PMM formulation with roof-top basis functions [21]. Moreover, once a promising candidate has been found by the GA, a refinement process has been carried out by using CST to further enhance the shape or tune the metamaterial performance. In our optimization process, the GA is encoded to pursue the spectral filter with the widest possible bandpass that respects the aforementioned constraints. In our study, we considered at first some canonical shapes such as a slot ring and a slot-cross and then, in order to explore promising new shapes for the unit cell of the metamaterial we have imposed some ad hoc design constraints to the GA routine determined by our fabricating process. In particular, we have forced the unit cell reported in Fig. 6(b) to have connections with adjacent elements, that is, we imposed some '0' along the perimeter with the aim to obtain a periodic element with an extension greater than the lattice periodicity T_x (Fig. 6(c)). It is important to underline that we have searched for the best performance of each filter in terms of the desired center frequency of the bandpass filter but also under the constraint in terms of available values of the substrate thickness as well as the resolution in the printing process of the periodic surface.

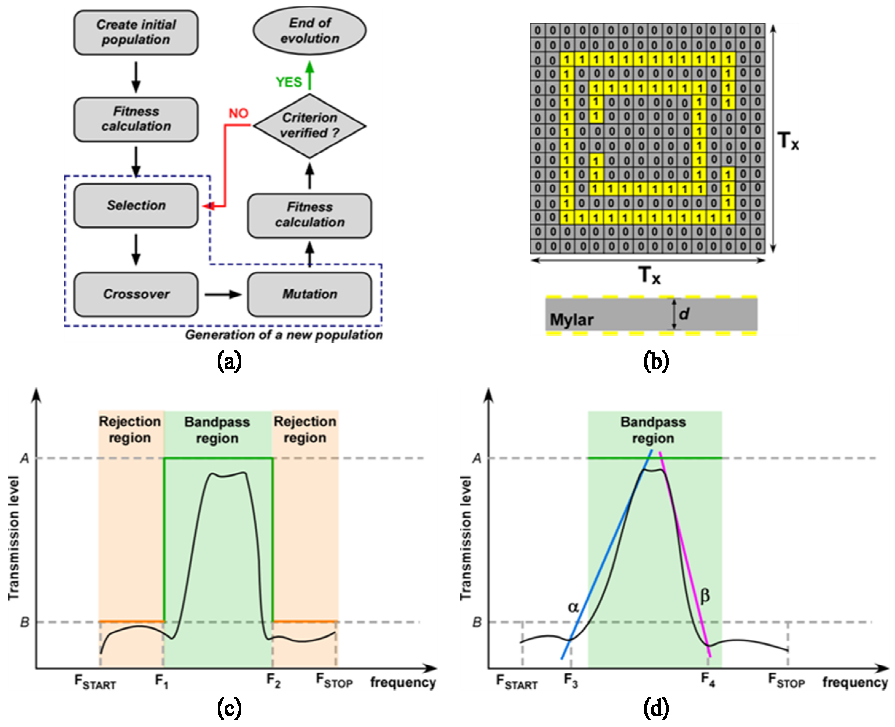

Fig. 5. (a) Flow chart of the genetic algorithm optimization (b) The MDM configuration to be optimized: stack up comprising a periodic surface printed on each side of a Mylar dielectric substrate and binary encoding of the unit cell. Example of the mask employed for the optimization of the frequency response of (c) the broadband passband filter and (d) of the sharp band-edge transition filter.

#162148 - $15.00 USD Received 27 Jan 2012; revised 1 Mar 2012; accepted 13 Mar 2012; published 19 Mar 2012

4.2 Ultra-broad bandpass and sharp-transition bandpass filter*s*

Applying the requirement of the maximum fractional bandwidth in our GA-based optimization process, we successfully obtain the MDM meandered slot, an ultra-broad bandpass filter as shown in Fig. 6(a). Figure 6 (b) presents the OM image of the fabricated MDM meandered slot, whose translation vectors are $t_1 = 64\mu m\ \hat{x}$ and $t_2 = 64\mu m\ \hat{y}$ in the Cartesian coordinate system and the simulated and measured transmittance spectra. It is evident to observe a THz bandpass filter with an ultra-broad fractional bandwidth up to 82.2%, which is, to the best of our knowledge, the broadest presented so far in the THz regime.

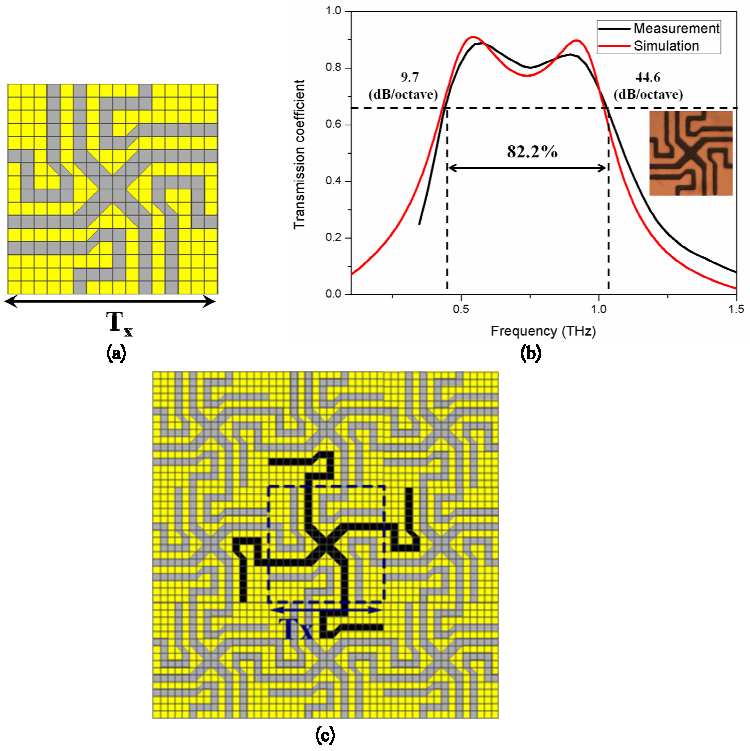

Fig. 6. (a) The unit cell of the MDM meandered slots; T_x = 64 μm and slot width = 4 μm. (b) The transmittance spectra of the MDM meandered slot. The inset shows the OM image of the fabricated sample. (c) The overall footprint of the periodic meandered shape (highlighted in black) exceeds a square of side *Tx* (dashed blue line).

In addition to ultra-broad bandpass filter, we also employ our GA process to sharpen the band-edge transition. The optimized pattern of the sharp-transition bandpass filter appears the MDM Jerusalem cross-slot array, whose translation vector is $t_1 = 48\mu m\ \hat{x}$ and $t_2 = 48\mu m\ \hat{y}$ in the Cartesian coordinate system and the geometric parameters are detailed in Fig. 7(a). As clearly displayed in Fig. 7(b), we successfully demonstrated a THz filter with sharp band-edge transitions, 25.5 dB/oct for the lower band-edge transition and 58.3 dB/oct for the upper band-edge transitions respectively. In summary, by hybridizing multiple resonances in our MDM metamaterials and optimizing their geometry, here we realize two more remarkable THz bandpass filters with ultra-broad fractional bandwidth (i.e., MDM meandered slots) and sharp band-edge transition (i.e., MDM Jerusalem cross slots). All simulation and measurement results are in excellent agreement. Moreover, the distribution of the induced currents (not shown here) of the other two MDM structures, meandered slot and Jerusalem cross slots, are

#162148 - $15.00 USD Received 27 Jan 2012; revised 1 Mar 2012; accepted 13 Mar 2012; published 19 Mar 2012

also simulated, and we are able to elucidate the mechanisms of forming the broad bandpass behaviors by means of the explanations in Section 3.

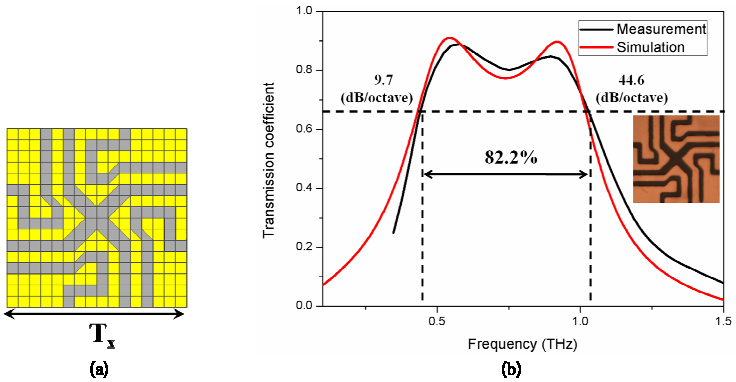

Fig. 7. (a) The unit cell of the MDM Jerusalem cross slots; T_x = 48 μm, W = 4 μm, S = 12 μm, M = 37 μm, N = 33 μm, L = 45 μm, H_{cap} = 20 μm, and J_{cap} = 10 μm. (b) The transmittance spectra of the MDM Jerusalem cross slot. The inset shows the OM image of the fabricated sample.

We introduced the misalignment in all MDM structures on purpose, to inspect the influence of misalignment in our simulation as shown in Fig. 8. We found that the misalignment contributes almost no effect on their performance. In fact, we even increased the misalignment along both x- and y- directions to the maximum (i.e., half period), the worst case of the misalignment, and the simulated results reveal that the corresponding frequencies results remain the same, and the transmission coefficients show a small offset less than 1.5%. In addition to our simulation, from a theoretical point of view [21] the analysis of two cascaded infinite periodic surface of the same periodicity can be seen as the product of their scattering matrices. The scattering matrix of each infinite surface does not depend on the relative shift between them, and therefore the overall result is not influenced by this shift. Moreover, during the fabrication process we can carefully control the translation misalignment with the accuracy less than five percent, which is small enough to neglect its effect.

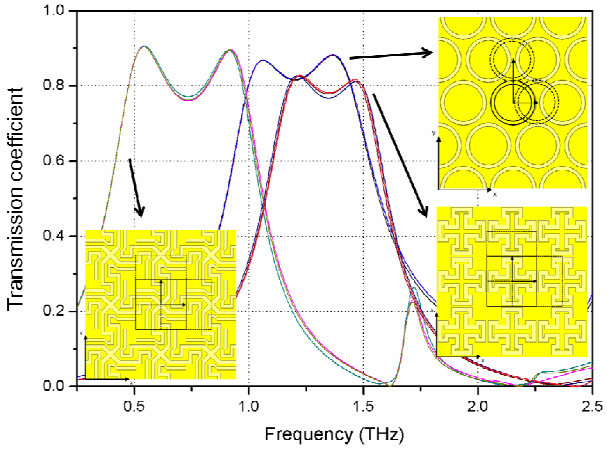

Fig. 8. The simulated results of misalignment effect. We misaligned two layers along both x- and y-directions on purpose. Even for the worst case (i.e., the misalignment is up to half periodicity along both x- and y-directions), the corresponding frequencies results remain the same, and the transmission coefficients show a small offset less than 1.5%.

#162148 - $15.00 USD Received 27 Jan 2012; revised 1 Mar 2012; accepted 13 Mar 2012; published 19 Mar 2012

5. Conclusions

In this work, we presented three monolithic metamaterial-based THz bandpass filters of the skewed circular slot rings, meandered slots and Jerusalem cross slots beyond conventional ones. After scrutinizing the distribution of the induced currents in these three THz bandpass filters, we found out that their metal-dielectric-metal structures support multiple resonances of electric dipole, magnetic dipole, and standing-wave-like modes, respectively. By hybridizing these individual resonance modes to activate the trapped-mode resonances, we were able to realize the excellent performance of broad bandwidth and sharp band-edge transition. In addition, we further optimized the performance of the skewed circular slot rings, for example, broader bandwidth and sharper band-edge transition, by means of our ad hoc genetic algorithm (GA) and periodic method of moments (PMM), leading to two more THz filters of the meandered slots and Jerusalem cross slots, respectively. With the meandered slots, we achieved an ultra-broad 3dB fractional bandwidth up to 82.2%, which is, to the best of our knowledge, the broadest presented so far in the THz regime; with the Jerusalem cross slots, we demonstrated a sharp band-edge transition of 58.3 dB/octave. Resting on the method of hybrid multiple resonances and the ad hoc GA and PMM, our work promises the capability of designing the THz metamaterials with the desired behaviors, paving a way toward widening the area of THz applications, such as material recognition in security systems, imaging, absorbers and others.

Acknowledgments

The authors would like to acknowledge the financial support from the National Science Council in Taiwan (98-2112-M-007-002-MY3, 99-2923-M-007-003-MY2, 99-ET-E-007-002-ET, 100-ET-E-007-002-ET, 100-2120-M-002-008 and 100-2120-M-010-001) and the Bilateral Projects Program of the National Research Council in Italy.

#162148 - $15.00 USD Received 27 Jan 2012; revised 1 Mar 2012; accepted 13 Mar 2012; published 19 Mar 2012